



## Cu@LaNiO<sub>3</sub> based nanocomposites in TWC applications

G. Perin <sup>a</sup>, J. Fabro <sup>b</sup>, M. Guiotto <sup>b</sup>, Q. Xin <sup>c</sup>, M.M. Natile <sup>a,d</sup>, P. Cool <sup>c</sup>, P. Canu <sup>b</sup>, A. Glisenti <sup>a,d,\*</sup>

<sup>a</sup> Dept. of Chemical Sciences, University of Padova, Via F. Marzolo, 1, 35131, Padova, Italy

<sup>b</sup> Dept. of Industrial Engineering, University of Padova Via F. Marzolo, 9, 35131, Padova, Italy

<sup>c</sup> Laboratory of Adsorption and Catalysis, Department of Chemistry, University of Antwerp, Universiteitplein 1, 2610 Wilrijk, Belgium

<sup>d</sup> CNR-ICMATE, INSTM Via F. Marzolo, 1, 35131, Padova, Italy

### ARTICLE INFO

#### Article history:

Received 26 October 2016

Received in revised form 17 February 2017

Accepted 19 February 2017

Available online 22 February 2017

#### Keywords:

TWC

PGM-free catalysts

NO reduction

LaNiO<sub>3</sub>-based nanocomposites

Ammonia-Driving Deposition Precipitation (ADP)

### ABSTRACT

Several nanocomposites of the type CuO/LaNiO<sub>3</sub> (Cu@LaNiO<sub>3</sub>) have been developed for application as noble metal free catalysts in TWC. The nanocomposites have been obtained by depositing copper oxide on lanthanum nickelate. The supporting perovskite has been prepared by means of the citrate route; copper, in contrast, was deposited by means of an innovative procedure: ammonia driven deposition precipitation method (ADP) optimized for deposition on perovskites. The nanocomposites have been developed based on the catalytic activity of LaNiO<sub>3</sub> in oxidation and reforming reactions and of copper in reduction reactions. Nanocomposition is thus used to deposit a highly dispersed active specie (CuO) on an active support (LaNiO<sub>3</sub>) with the aim of building catalytic functionality.

The obtained nanocomposites have been characterized by means of XRD, XPS, SEM, TPR, BET, EDX, and ICP and the obtained results are correlated to the amount of copper deposited and to the reactivity. The reactivity was studied first in two model reactions, CO oxidation and CO assisted NO reduction, in order to investigate the role played by the different species. Moreover, the reactivity under real conditions, i.e. with a complex mixture reflecting the actual automotive exhaust composition, was considered to evaluate the real applicability. Finally, high-temperature deactivation was investigated. XPS reveals that the deposition of copper oxide affects the surface composition of the nanocomposites; the XRD, SEM, and TPR results confirm that CuO is deposited on the LaNiO<sub>3</sub> surface and no diffusion below surface is observed. CuO species are deposited both as highly dispersed phase and as bigger particles; the relative amount of these phases depends on the total amount of copper deposited. The reactivity in the CO oxidation reaction is not significantly affected by the copper deposition. In contrast the reactivity in NO reduction is strongly enhanced by the presence of highly dispersed copper species. Activity tests with mixture reflecting actual automotive exhaust, reveal an enhancement in CO oxidation, but no NO decomposition at stoichiometric conditions. Complete NO reduction is achieved at rich conditions; also, hydrocarbons reforming reactions typically occurring at substoichiometric O<sub>2</sub>, with CO and H<sub>2</sub> production, are less supported, preserving the activity in NO reduction. Finally, the high-temperature aging test confirmed an interesting stability of catalytic activity.

© 2017 Elsevier B.V. All rights reserved.

### 1. Introduction

The pollutants abatement from auto exhaust gases is one of the objectives of environmental catalysis. Great success has been achieved by applying three-way catalysts (TWC) [1]. In the three-way catalysts the simultaneous oxidation of CO and unburned hydrocarbons (HCs) and reduction of NO has to be achieved. Moreover, NO should be selectively converted to N<sub>2</sub> rather than NO<sub>2</sub>,

NH<sub>3</sub> or N<sub>2</sub>O, that are toxic or greenhouse-gases. The high performance of TWC is mainly due to the presence of noble metals as Pt, Pd and Rh. These elements are characterized by a high cost and most of them are considered critical raw materials. Taking into account the limited supply and high cost and the need to fulfill the highly restrictive requirements imposed to TWC a lot of effort is focused on the development of high performance noble metal-free catalysts. Recently, special attention has been paid to the perovskite-type mixed oxides due to their excellent redox properties, early pointed out by Libby [2], low cost and environmental impact, high diffusion.

Perovskites are mixed oxides characterized by high compositional and structural versatility allowing the incorporation of different catalytically active cations in their structure. Moreover,

\* Corresponding author at: Dept. of Chemical Sciences, University of Padova, Via F. Marzolo, 1, 35131 Padova, Italy.

E-mail address: [antonella.glisenti@unipd.it](mailto:antonella.glisenti@unipd.it) (A. Glisenti).

perovskites are known to be capable of stabilizing highly dispersed nanoparticles deposited on their surface. Among the perovskites, lanthanum nickelate-based ones have been extensively studied in literature for steam reforming [3,4], dry reforming of methane [5–25], autothermal reforming of methane [26,27], ethanol [3,28], toluene [29,30], partial oxidation of methane [31–34] and of glycerol [35–37]. Nickelates use in CO oxidation and De-NOX processes was scarcely considered [38–40] and the possible use in TWC was never investigated.

Copper containing catalysts are used in a lot of different reactions among which steam reforming and oxidative steam reforming of alcohols [41], preferential CO oxidation [42–44], methanol synthesis [45,46]. In all these reactions copper plays a fundamental role and the best performance is obtained when it is present in a highly dispersed form [41]. Recently [47] we observed that the presence of copper increases the activity of LaCoO<sub>3</sub> in NO reduction suggesting a different role of the two transition cations in the reactivity and a synergic effect. On the basis of the reactivity of copper in NO reduction and of nickel in oxidation and steam reforming, we decided to develop nanocomposite systems in which copper oxide is highly dispersed on the surface of LaNiO<sub>3</sub> with the intent of adding functional catalytic activity. Copper containing composites differing for the supports (ZnO, ZrO<sub>2</sub>, SiO<sub>2</sub>, CeO<sub>2</sub>), preparation procedure (impregnation, precipitation, etc), composition, activation treatments (reduction, as an example), are observed to show a different activity and selectivity [48–65]. Among the supports, perovskite based oxides can be particularly promising [66]. Perovskite structures can stabilize copper atoms avoiding their migration and particles sintering.

In the present contribution several nanocomposites characterized by increasing amount of copper oxide deposited on LaNiO<sub>3</sub> have been prepared and tested for TWC.

The perovskite was prepared by means of the citrate method whereas for the copper we applied an innovative ammonia based impregnation method. The so-called ammonia driven deposition precipitation (ADP) method was first reported by Guo et al. as a simple and efficient preparation approach for silica supported copper catalysts [67]. The formation of copper tetra-ammonia complex [Cu(NH<sub>3</sub>)<sub>4</sub>(H<sub>2</sub>O)<sub>2</sub>]<sup>2+</sup> provides an excellent steric hindrance between the individual Cu ions. The overall result after the calcination is a well dispersed CuO phase upon the material. In the current paper, we optimize and adapt the existing method in order to enhance the dispersion degree on perovskite surfaces. For comparison, a Cu loaded LaNiO<sub>3</sub> catalyst was also prepared by using the conventional wet impregnation (WI) method.

The obtained nanocomposites are characterized by means of X-Ray Diffraction (XRD), X-Ray Photoelectron Spectroscopy (XPS), Scanning Electron Microscopy (SEM), Energy Dispersive X-Ray (EDX) Spectroscopy, Temperature Programmed Reduction (TPR), BET, Inductive Coupled Plasma Optical Emission Spectrometry (ICP-OES), and Transmission Electron Microscopy (TEM), and the obtained results are related to the observed catalytic activity.

The catalytic activity was investigated in two model reaction, CO oxidation and CO assisted NO reduction, to help understand-

ing the role played by the different species, and with a complex mixture formulated in order to simulate the real emission of an engine to evaluate the catalytic behavior under real conditions. It is important, in fact, to observe that the reactivity can significantly change in all these environments. Furthermore, catalysts durability has been investigated, because of its relevance for actual applicability. One of the challenges of the industrial application is the thermal degradation, that may cause a sintering of metal oxides and consequently a loss in catalytic surface area [68]. For this reason, thermal deactivation has been studied by exposing the catalysts to an aging treatment alternating low and high temperatures, up to 800 °C.

## 2. Experimental

### 2.1. Synthesis of LaNiO<sub>3</sub> support

The perovskite support has been synthesized with the conventional citrate route [69], starting from La<sub>2</sub>O<sub>3</sub> (Sigma-Aldrich 99.9%), NiO (Acros 99%). Citric acid monohydrate (Sigma-Aldrich ≥99.0%) was added to the precursors solution under vigorous stirring. The solution was heated at 80 °C in a water bath to promote solvent evaporation and obtain a wet-gel, which was then treated at 400 °C for 2 h in air to decompose the organic framework. The ash-like material was finally grinded and calcined in air at 750 °C (heating rate 6 °C/min) for 6 h to obtain the desired perovskite phase.

### 2.2. Synthesis of the Cu@LaNiO<sub>3</sub> nanocomposites by ADP and by WI

Copper was deposited via ammonia driven deposition precipitation method, which was optimized for perovskites. Typically, an appropriate amount of Cu precursor (copper nitrate, Cu(NO<sub>3</sub>)<sub>2</sub>·3H<sub>2</sub>O, >99%, Merck) was dissolved in 10 mL of de-ionized water containing the support material in order to achieve a final Cu loading of 10, 15, 20 and 30 wt%. Consequently, ammonium hydrate (NH<sub>4</sub>OH, 28–30%, Sigma Aldrich) has been added into the mixture to gain a molar Cu/NH<sub>3</sub> ratio of 1/6. The suspensions were then stirred for 48 h at room temperature, followed by a drying step at 60 °C overnight. Finally, the dried samples were calcined at 550 °C (heating rate 1 °C/min) for 8 h. The synthesized catalysts were denoted as 10 CLN, 15 CLN, 20 CLN and 30 CLN, according to the copper loading.

As reference, two Cu@LaNiO<sub>3</sub> samples containing 15 and 30 wt% of Cu were also prepared by the conventional wet impregnation method. In this method LaNiO<sub>3</sub> was added into a 25 mL solution containing a required amount of Cu(NO<sub>3</sub>)<sub>2</sub>·3H<sub>2</sub>O (>99%, Merck) so that the metal loading reached 15 and 30 wt.% in the final catalyst. The mixture was stirred at room temperature for 48 h and dried at 60 °C overnight. Finally, the solid was calcined at 550 °C, (heating rate 1 °C/min) for 6 h.

The prepared samples are summarized in Table 1, as well as the specific surface areas, the pore volumes and pore dimensions.

**Table 1**

BET Specific Surface Area, Pore Volume and Dimension as a function of the composition (nominal and ICP measured).

Sample <sup>a</sup>	Deposition method	Sample name	Cu/Ni <sup>a</sup>	Cu/Ni (ICP)	S <sub>BET</sub> (m <sup>2</sup> /g)	Vpore (cc/g)	D <sub>p</sub> (nm)
LaNiO <sub>3</sub>	–	LaNiO <sub>3</sub>			7.6	0.027	14.4
10% wt. Cu on LaNiO <sub>3</sub>	ADP	10 CLN	0.39	0.35	8.1	0.029	14.5
15% wt. Cu on LaNiO <sub>3</sub>	ADP	15 CLN	0.58	0.57	8.3	0.029	13.9
20% wt. Cu on LaNiO <sub>3</sub>	ADP	20 CLN	0.77	0.73	7.9	0.035	17.9
30% wt. Cu on LaNiO <sub>3</sub>	ADP	30 CLN	1.16	1.13	10.5	0.039	14.8
15% wt. Cu on LaNiO <sub>3</sub>	WI	15 CLN WI	0.58	0.55	6.7	0.025	13.8
30% wt. Cu on LaNiO <sub>3</sub>	WI	30 CLN WI	1.16	1.06	7.8	0.023	13.4

<sup>a</sup> = from precursors' weighted amounts.

**Table 2**

Feed composition used for the catalytic measurements.

Inert	CO <sub>2</sub>	H <sub>2</sub> O	O <sub>2</sub>	CO	NO	H <sub>2</sub>	CH <sub>4</sub>	C <sub>3</sub> H <sub>6</sub>	C <sub>3</sub> H <sub>8</sub>	Δ <sup>a</sup>	m <sub>cat</sub>	Flow	GHSV <sup>b</sup>	
(balance)	%	%	%	%	%	%	ppm	ppm	ppm	—	mg	S ml/min	1/h	
Ar	—	—	—	4	4	—	—	—	—	—	40	100	150000	
Ar	—	—	2	4	—	—	—	—	—	1.0	Stoich	40	100	150000
He	15	10	0.777	0.7	0.1	0.233	230	450	230	1.0	Stoich	200	200	60000
He	15	10	0.609	0.9	0.1	0.300	300	600	300	0.6	Rich	200	200	60000
—														

<sup>a</sup> Δ = O<sub>2</sub> fed/O<sub>2</sub> stoichiometric = ([O<sub>2</sub>] + 0.5 [NO])/(0.5 [CO] + 0.5 [H<sub>2</sub>] + 2 [CH<sub>4</sub>] + 4.5 [C<sub>3</sub>H<sub>6</sub>] + 5 [C<sub>3</sub>H<sub>8</sub>]).<sup>b</sup> For GHSV we assumed a bulk density of 1 g/ml for all the powders.

### 2.3. Characterization

X-ray diffraction patterns were collected with a Bruker D8 Advance automatic diffractometer, with Cu K $\alpha$  wavelength ( $\lambda = 0.154$  nm) at a voltage of 40 kV and a current of 40 mA.

X-ray photoelectron spectroscopy was carried out by means of a ParkinElmer PHI 5600ci Multi Technique System, using AlK $\alpha$  radiation (1486.6 eV) working at 250 W. The spectrometer was calibrated by assuming the binding energy (BE) of the Au 4f<sub>7/2</sub> line to be 84.0 eV with respect to the Fermi level.

Both extended spectra (survey – 187.85 eV pass energy, 0.5 eVstep<sup>-1</sup>, 0.05 sstep<sup>-1</sup>) and detailed spectra (for La 3d, Cu 2p, Ni 2p, O 1s and C 1s – 23.5 eV pass energy, 0.1 eVstep<sup>-1</sup>, 0.1 sstep<sup>-1</sup>) were collected. The standard deviation in the BE values of the XPS line is 0.10 eV. The atomic percentage, after a Shirley-type background subtraction [70] was evaluated by using the PHI sensitivity factors [71]. The peak positions were corrected for the charging effects by considering the C 1s peak at 285.0 eV and evaluating the BE differences [72].

Field emission-scanning electron microscopy and energy dispersive x-ray spectroscopy measures were carried out on a Zeiss SUPRA 40VP. Both morphological and compositional analyses were carried out setting the acceleration voltages at 20 kV.

The TPR measurements were carried out with an Autochem II 2920 Micromeritics, equipped with a TCD detector in a quartz reactor by using 50 mg of sample and heating from RT to 900 °C at 10 °C/min under a constant flow of H<sub>2</sub> at 5% in Ar (50 ml min<sup>-1</sup>). TPR samples were previously outgassed with He (50 ml min<sup>-1</sup>) at RT. The surface area of all samples was determined by Quantachrome Quadrasorb SI automated gas adsorption system. The measurements were carried out at liquid nitrogen temperature (77 K). The specific surface area was calculated using the Brunauer-Emmet-Teller (BET) equation. Prior to N<sub>2</sub>-sorption, all samples were degassed at 200 °C for 16 h. Inductively coupled plasma optical emission spectrometry was performed with a Perkin Elmer Optima 4200 Dual View. The samples for ICP analysis were prepared by dissolving the powder (about 20 mg exactly weighted) in a solution of 10 mL of HCl (Sigma-Aldrich ≥ 37%) and 10 mL HNO<sub>3</sub> (Sigma Aldrich, ≥ 65%) under stirring at about 80 °C for 2 h.

TEM analysis was performed with Tecnai G2 (FEI) transmission electron microscope operating at 100 kV. Images were captured with a Veleta (Olympus Soft Imaging System) digital camera. Samples dispersed in ethanol were drop cast on carbon-coated grids (400 mesh Cu).

### 2.4. Catalytic tests

Two series of activity tests were carried out, at atmospheric pressure. All the inlet composition and GHSV data are summarized in Table 2. The first set of measurements is based on simplified mixtures and performed in a glass reactor (6 mm ID) with a fixed bed of powders; the temperature was monitored by a thermocouple right upstream of the bed. In this configuration we studied the NO + CO and CO + O<sub>2</sub> reactions, using a stoichiometric mixture. The

inert carrier was always Ar. The flows were controlled by thermal mass flow meters (Vögtlin Instruments). The temperature of the bed was raised from RT to 400 °C and the composition of the gas mixture was measured by GC (Agilent 7890A) equipped with a TCD detector and 13X (60/80 mesh, 1.8 m) and Porapak Q (1.8 m) columns. FTIR(Bruker Tensor 27–32 scans at a resolution of 1 cm<sup>-1</sup>) was used to check for possible N<sub>2</sub>O, NO<sub>2</sub> and NH<sub>3</sub> formation.

The concentration of reactants and the space velocity used in the first set of activity test is quite larger than typical automotive exhaust conditions. The purpose is a consistent pre-screening of catalytic materials, at conditions frequently used in the Literature. It must be underlined that ignition temperature may differ from the results of actual feed concentrations and space velocities, also because of a significant adiabatic temperature rise (approaching 600 °C). While more realistic conditions have been addressed in the second set of measurements, the first set remains self-consistent, to rank the activity of the synthesized materials.

The second set of activity measurements approaches the actual conditions of an automotive exhaust using a feed mixture that simulates the real one (detailed in Table 2), in order to verify the applicability of the new materials as three way catalysts. Note that 10% steam was always fed, reflecting actual conditions, quite challenging for the catalysts. A quartz flow reactor, 8 mm ID, was used. The experimental set-up has been already described [73]. The gas mixtures were measured by GC (Agilent 7820) equipped with Porapak Q and MS5A packed columns in series; both TCD and FID detectors were used. The GC is online with the reactor gas outlet and programmed to continuously sample the mixture, so that measurements can be collected at approx. 0.1 sample/min. A direct-access, 0–200 amu mass spectrometer (Hiden QID-20) was used to measure NO. The analysis with the MS is almost continuous (0.5–1 sample/min) and it was in parallel with the GC. The flows were controlled by mass flow meters (Brooks and Bronkhorst). The stoichiometric O<sub>2</sub> amount is based on all the fuels and the amount expected from NO conversion to N<sub>2</sub> and O<sub>2</sub>.

The standard testing sequence for the second set of measurements was (1) heating up the catalyst at 10 °C/min to 600 °C in air, (2) 2 h of pre-conditioning at 600 °C in air, (3) 2 h of conditioning at 600 °C with the reacting mixture, (4) slow temperature decrease (−2 °C/min) to measure the catalyst activity at different temperatures. It has been verified that the selected cooling rate of −2 °C/min is sufficiently slow to achieve steady-state operation of the catalyst, at each temperature scanned.

Aging protocol consisted in different steps alternating low and high temperatures, up to 800 °C. The real-conditions stoichiometric mixture was always fed throughout the whole sequence. The first step was equivalent to the standard testing sequence. Temperature was reduced from 600 °C to ambient, as in step (4) above. In the second thermal cycle the catalyst was rapidly (15 °C/min) brought to 700 °C and kept for 3 h. After cooling down to 600 °C, step (4) of the standard was performed. Then, the catalyst was rapidly (15 °C/min) re-heated to 800 °C and treated for 3 h at 800 °C under the same, real stoichiometric conditions. Finally, it was cooled to 600 °C to repeat step (4) of the standard testing sequence. Total aging treatment

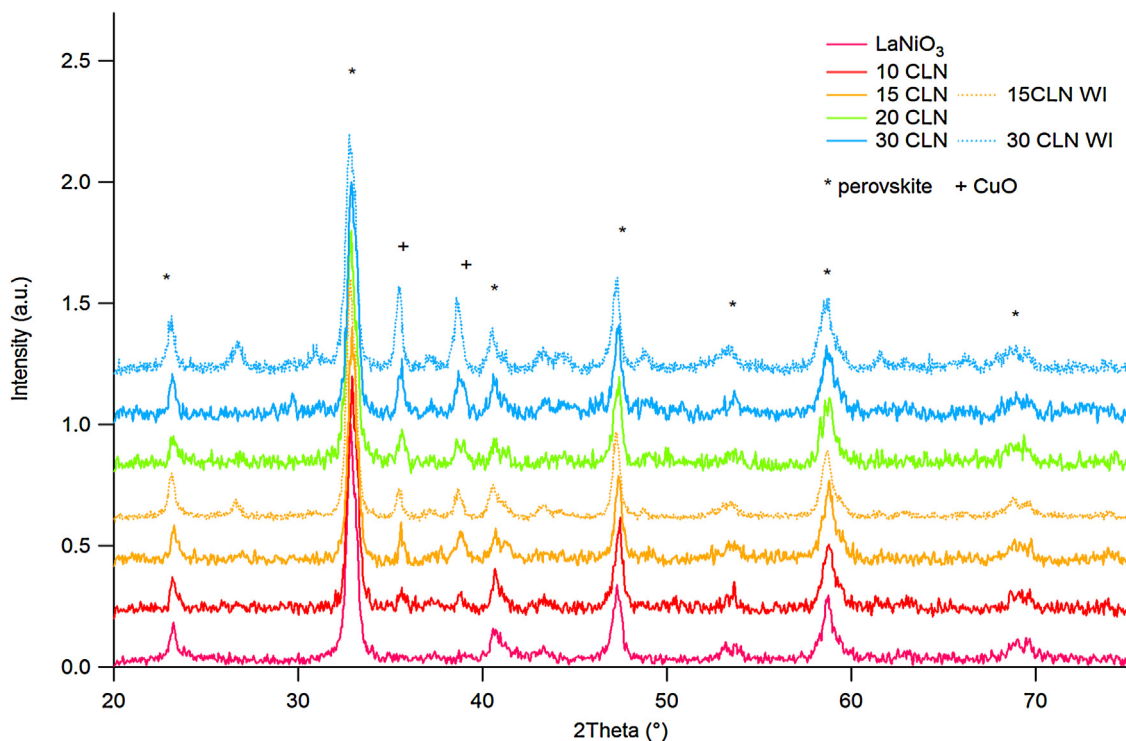


**Fig. 1.** XRD patterns of the supporting LaNiO<sub>3</sub> and of the Cu@LaNiO<sub>3</sub> nanocomposites (CLN) obtained by ADP and by WI.

took approx. 30 h. The catalytic activity was evaluated on the fresh sample and after each high-temperature treatment.

### 3. Results and discussion

#### 3.1. Chemical, structural, and morphological characterization

XRD patterns of LaNiO<sub>3</sub>, 10 CLN, 15 CLN, 20 CLN and 30 CLN are shown in Fig. 1. Reflections at 2θ angles of 23.2, 32.9, 40.6, 47.4, 53.6, 58.7 and 68.9° were assigned to rhombohedral LaNiO<sub>3</sub> perovskite (JCPDS 01-079-2450); reflections at 2θ angles of 35.6 and 38.7° were assigned to cubic copper oxide (JCPDS 01-072-0629).

The typical reflections of cubic copper oxide are evident in addition to those of the LaNiO<sub>3</sub> perovskite; no side phases have been observed. Moreover, it is possible to observe an intensity enhancement in CuO signals increasing with the amount of copper oxide deposited. Noteworthy, no shift of the perovskite peaks with increasing of copper oxide content is detected: this suggests that Cu does not enter inside the perovskite unit cell. Literature data suggest that this is possible when treating at higher temperature (>700 °C) [74].

The deposition of CuO on the LaNiO<sub>3</sub> is also confirmed by the TEM images (Fig. 2) reported for 10 CLN and 30 CLN; in the 10 CLN sample few particles around 20–30 nm are observed; with increasing the deposited amount of copper numerous small particles appear in addition to the big ones.

#### 3.2. X-Ray photoelectron spectroscopy (XPS)

XPS spectra are reported in Fig. 3. The La3d<sub>5/2</sub> peak (Fig. 3) is centred at 834.4–834.7 eV and has the typical structure (with a shake-up contribution at 837.9–838.2 eV) expected for lanthanum(III) [75–77]. The broadened shape of La3d<sub>5/2</sub> peak suggests the presence of two contributions, which are assigned to perovskite (833.4–833.6 eV) and to La(OH)<sub>3</sub> and LaOOH species (834.6–834.9 eV) [78–81].

Copper deposition seems to induce a higher lanthanum hydroxylation. Ni2p spectra have a difficult interpretation due to La3d<sub>3/2</sub> shake-up structure superposition signal. However, both the peak position (854.9–855.2 eV) and the presence of shake-up signals (861.9–862.6 eV and 879.7–880 eV) agree with the presence of Ni(II) in the outmost layers [82,83].

The spectra of Cu2p<sub>3/2</sub> (Fig. 3) reveal the presence of Cu(II), as it is possible to observe from both peak binding energy (933.3–933.9 eV) and shake-up contributions (942.3–942.9 eV) [84,85], this is consistent with the presence of CuO observed in XRD measurements. No significant variation of shake-up intensities with amount of deposited copper was observed; this is an important result suggesting that Cu is always present mainly as Cu(II), and not in lower oxidation states as sometime observed.

The shape of O1s peak (Fig. 3) suggests the presence of two contributions at least due to perovskite lattice oxygen species (529–529.5 eV) [86], and to oxydrilic and carbonatic groups (531.2–531.8 eV) [79,84]. The less evident perovskitic oxygen signal in the 20 CLN and 30 CLN samples is in agreement with the presence of a higher amount of hydroxide and carbonate species.

The atomic compositions obtained by means of XPS and EDX are reported in Table 3 and compared with the nominal ones, determined by the weighted amounts, while ICP composition is reported in Table 1 (Section 2.2); in order to emphasize the cation segregation phenomena, the composition determined without considering oxygen is also reported.

The XPS atomic composition shows, in general, a surface enrichment in oxygen due to the presence of hydroxides and carbonates; this is a surface phenomenon that is a lot less evident from the EDX data.

The amount of atomic oxygen seems slightly less evident in the sample 15 CLN. Lanthanum is significantly surface segregated in the supporting LaNiO<sub>3</sub> (La/Ni atomic ratio = 2.4) but this behaviour is less evident in the nanocomposites. Moreover, lanthanum segregation is a surface specific phenomenon as suggested by the comparison with the La/Ni atomic ratios obtained by means of EDX

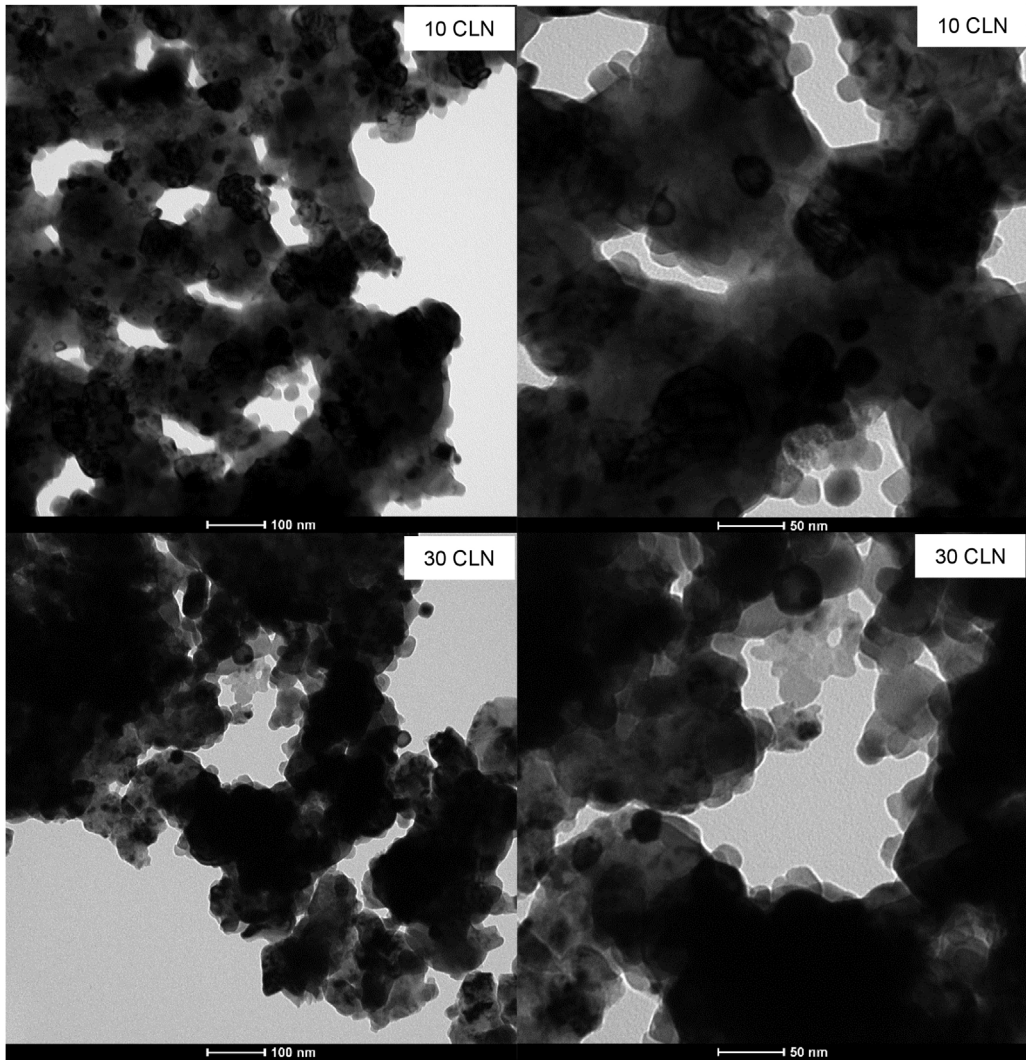


**Fig. 2.** TEM images of the Cu@LaNiO<sub>3</sub> nanocomposites with lower (10 CLN) and higher (30 CLN) copper content, obtained by ADP.

that all range around 1. Copper is always present in slightly lower amount with respect to the nominal values in XPS composition; the only exception is when considering the XPS cations composition determined for 10 CLN. Also this is a surface phenomenon as confirmed by the ICP compositions (**Table 1**, Section 2.2), which are identical to the nominal ones.

The spectra obtained for the nanocomposites prepared by WI do not show relevant differences with the corresponding ADP ones but a slightly more evident presence of oxides (Cu, La) and hydroxides. As for the WI samples, the XPS atomic compositions reveals a lower amount of oxygen, suggesting a grafting mechanism that involves the interaction between supporting and supported hydroxide groups. A higher amount of Ni seems also to characterize the WI samples.

The SEM images (Fig. S1) reveal a globular morphology for the supporting LaNiO<sub>3</sub>; the particles, characterized by a diameter smaller than 100 nm, are grouped forming a rather porous and homogeneous morphology, which is not strongly modified by the deposition of copper. Only in the 30 CLN sample some more massive structure is visible. The comparison between the images obtained for the ADP and WI samples does not show significant differences.

### 3.3. Temperature programmed reduction

#### 3.3.1. LaNiO<sub>3</sub>

The H<sub>2</sub>-TPR profile of the unloaded LaNiO<sub>3</sub> is presented in **Fig. 4**. Based on the literature studies [13,15], mainly two reduction stages can be distinguished: the first one, around 400–440 °C, corresponding to the reduction of Ni(III) to Ni(II) and the higher temperature one (530–590 °C) to the reduction of Ni(II) to Ni(0). Gallego et al. [13,15] by means of in-situ XRD measurements, suggested that the reduction of LaNiO<sub>3</sub> proceeds through the following steps:

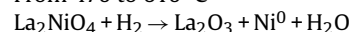
From 250 to 360 °C:



From 360 to 430 °C



From 470 to 610 °C



Valderrama et al. [14] suggested a first reduction ( $\alpha$ -peak at 360 °C) forming LaNiO<sub>2.7</sub> that is reduced at La<sub>2</sub>Ni<sub>2</sub>O<sub>5</sub> at 395 °C. Finally a peak at 540 °C ( $\beta$ -peak) corresponds to the reduction to elemental Ni and lanthanum oxide:

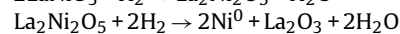
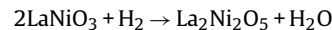


**Table 3**

XPS and EDX atomic compositions obtained for  $\text{LaNiO}_3$  and the  $\text{Cu@LaNiO}_3$  nanocomposites (CLN) obtained by depositing  $\text{CuO}$  by ADP and WI; inside brackets the atomic composition determined considering only the cations. The nominal compositions are reported for comparison.

Sample		La	Ni	Cu	O	La/Ni	Cu/Ni	Cu/La
$\text{LaNiO}_3$	XPS	18.4 (70.8)	7.6 (29.2)	–	74.0	2.4	–	–
	EDX	22.6	19.7	–	57.7	1.2	–	–
	Nominal	(53.4)	(46.6)		60.0	1.0		
		20.0 (50.0)	20.0 (50.0)					
10 CLN	XPS	12.9 (53.5)	6.1 (25.3)	5.1 (21.2)	75.9	2.1	0.8	0.4
	EDX	14.4	16.0	5.0	64.6	0.9	0.3	0.4
	Nominal	(40.7)	(45.2)	(14.1)	59.0	1.0	0.4	0.4
		17.0 (41.5)	17.0 (41.5)	7.0 (17.0)				
15 CLN	XPS	14.4 (44.4)	12.2 (37.7)	5.8 (17.9)	67.6	1.2	0.5	0.4
	EDX	14.9	16.5	10.4	58.3	0.9	0.6	0.7
	Nominal	(35.6)	(39.5)	(24.9)	58.0	1.0	0.6	0.6
		16.0 (39.0)	16.0 (39.0)	9.0 (22.0)				
15 CLN WI	XPS	14.1 (36.8)	17.3 (45.1)	7.0 (14.7)	61.6	0.8	0.4	0.5
	EDX	16.4	19.8	11.1	52.7	0.8	0.6	0.7
	Nominal	(34.7)	(41.9)	(23.4)	58.0	1.0	0.6	0.6
		16.0 (39.0)	16.0 (39.0)	9.0 (22.0)				
20 CLN	XPS	12.7 (50.0)	7.1 (28.0)	5.6 (22.0)	74.6	1.8	0.8	0.4
	EDX	14.8	14.3	9.2	61.7	1.0	0.6	0.6
	Nominal	(38.6)	(37.3)	(24.0)	58.0	1.0	0.8	0.8
		15.0 (35.7)	15.0 (35.7)	12.0 (28.6)				
30 CLN	XPS	10.9 (39.1)	8.6 (30.8)	8.4 (30.1)	72.1	1.3	1.0	0.8
	EDX	12.8	14.2	13.7	59.3	0.9	1.0	1.1
	Nominal	(31.4)	(34.9)	(33.7)	57.0	1.0	1.1	1.1
		14.0 (31.8)	14.0 (31.8)	16.0 (36.4)				
30 CLN WI	XPS	14.0 (35.3)	17.0 (43.0)	8.6 (21.7)	60.5	0.8	0.5	0.6
	EDX	15.7	17.9	15.2	51.3	0.9	0.9	1.0
	Nominal	(32.1)	(36.8)	(31.1)	57.0	1.0	1.1	1.1
		14.0 (31.8)	14.0 (31.8)	16.0 (36.4)				

The fitting procedure reveals the presence in the present case, of three contributions at 380, 424, and 541 °C; the comparison between the area ratios of corresponding peak (1:3.5:5.0) and the relative amount of  $\text{H}_2$  required for the different steps of the Gallego and Valderrama models, seem to suggest that both the paths are observed in our case (the consumptions suggest that about 40% of  $\text{LaNiO}_3$  follows the first way). The slight difference in the reduction temperatures could be due to the thermal history of the sample, as also revealed by S.M. de Lima et al. [87].

The comparison between the experimental and theoretical  $\text{H}_2$  consumptions reveals, moreover, that 90% of Ni is present as Ni(III). Stability and reversibility have been confirmed through TPR/TPO cycles (Supplementary material).

### 3.3.2. Cu-loaded $\text{LaNiO}_3$

After the copper deposition onto the perovskite material, additional peaks appeared around 280–290 and 315–325 °C (Fig. 4) and a shift of the nickel reduction temperatures is observed. In particular the peak attributed to the reduction of Ni(III), shifts from 420–430 °C to 350 °C whereas the signal corresponding to the Ni(II) reduction shifts from 540 to 560 °C. The effect of copper on catalysts' reducibility was revealed also by cobalt containing materials in which the presence of copper causes the decrease of reduction temperature [47,88]. Tien-Thao et al. [89,90], investigating a copper doped lanthanum cobaltite, hypothesize that under reducing

conditions copper diffuses towards the surface acting as a catalyst for hydrogen dissociation. In the present case, as revealed by XPS, the amount of copper on the surface is lower than the nominal and surface segregation can be enhanced under reduction conditions. Noteworthy, the enhancing effect of copper on reduction attitude is only observed for the Ni(III) reduction process. As already mentioned two new contributions are observed around 280–290 °C and 315–325 °C. The comparison with literature data [48,88–90] suggests the attribution of these signals to the reduction of copper (II). The TPR investigation carried out on a reference  $\text{CuO}$  revealed a Cu(II) to Cu(0) single step reduction (316 °C) consistent with the literature. This comparison allows to attribute the contribution at 315–325 °C to  $\text{CuO}$  reduction. The peak at 280–290 °C, is also attributed to  $\text{CuO}$  reduction: the shift towards lower temperatures (when compared with that at 315–325 °C) is probably due to the high degree of dispersion of copper oxide particles.

The comparison between the expected and measured  $\text{H}_2$  consumption reveals that the measured consumption is lower than the expected, consistently with the presence of cations in lower oxidation state (Ni(II), as an example, was observed in the supporting  $\text{LaNiO}_3$ ). Interesting observations derive from the comparison among the relative intensity of the different signals (determined by fitting) summarized in Table 4. The intensity ratio Peak 3/Peak 4 (i.e. Ni(III) to Ni(II) vs. Ni(II) to Ni(0)) significantly decreases with increasing copper loading suggesting that the copper depo-

**Table 4**

TPR H<sub>2</sub> consumption data determined on LaNiO<sub>3</sub> and on the nanocomposites (CLN) obtained by depositing CuO by ADP and WI; the consumption values are compared with the expected ones and the% contributions of the single signals are evaluated by fitting procedure.

	H <sub>2</sub> [mol/g] Measured	H <sub>2</sub> [mol/g] Expected <sup>a</sup>	Peak 1		Peak 2		Peak 3		Peak 4		Peak 5	
			T (°C)	(%)	T (°C)	(%)	T (°C)	(%)	T (°C)	(%)	T (°C)	(%)
LaNiO <sub>3</sub>	0.05399	0.0611					380424	10.536.7	541	52.8		
10 CLN	0.00596	0.00690	289	5.8	326	16.9	390	31.5	545	45.7		
15 CLN	0.00711	0.00728	297	14.7	326	14.8	405	39.9	555	30.6		
20 CLN	0.00695	0.00765	290	23.5	334	11.7	360	31.4	561	33.5		
30 CLN	0.00797	0.00836	280	25.6	315	11.1	351	36.9	526	25.6	622	0.8
15 CLN WI	0.00731	0.00728	292	2.3	372	25.6	397	41.4	546	30.7		
30 CLN WI	0.00790	0.00836	288	4.6	352	42.6	381	33.0	539	15.9	594	3.8

<sup>a</sup> The expected% of consumption determined considering Ni(III) and Cu(II).

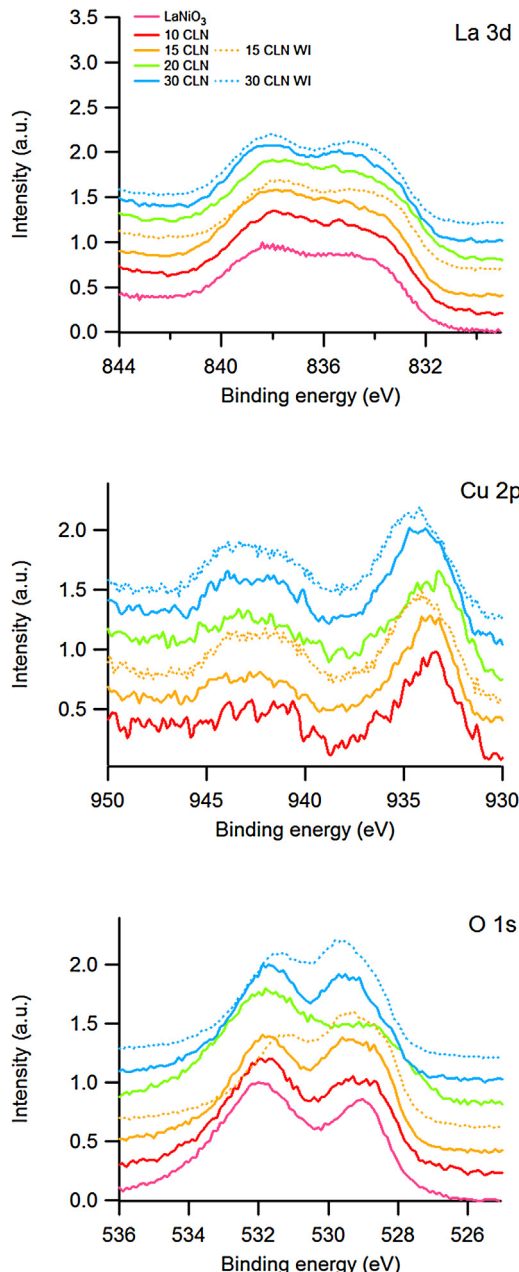


**Fig. 3.** XPS spectra of La3d<sub>5/2</sub>, Cu2p<sub>3/2</sub>, O1s, spectral regions observed for the Cu@LaNiO<sub>3</sub> (CLN) samples obtained by ADP and WI as a function of the increasing copper amount.

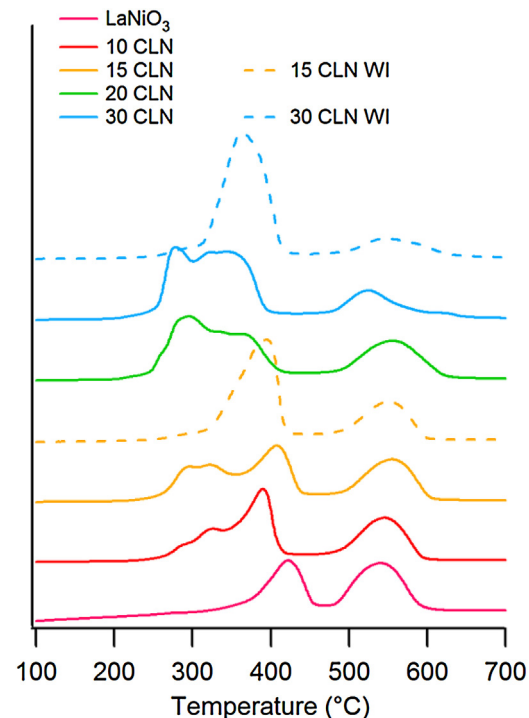


**Fig. 4.** H<sub>2</sub>-TPR profile of LaNiO<sub>3</sub> and of the Cu@LaNiO<sub>3</sub> (CLN) samples obtained by ADP and WI as a function of the increasing copper amount.

sition favours the Ni(II) to Ni(0) reduction at lower temperature. Focussing on the copper oxide reduction signals, the fitting results reveal that the intensity of the signal due to highly dispersed CuO (280–290 °C) increases from 10 CLN to 20 CLN whereas the one at 315–325 °C decreases suggesting that the increment of deposited copper oxide favours the formation of the highly dispersed CuO particles.

The TPR results of the WI samples show a high intensity of the signal attributed to poorly dispersed CuO (more than 40% in 30 CLN WI) confirming the validity of the ADP procedure for the deposition of highly dispersed CuO particles.

### 3.4. N<sub>2</sub>-Sorption data

N<sub>2</sub>-sorption isotherm of the samples indicates a type V isotherm with a H<sub>3</sub> type of hysteresis. This suggests the presence of slit-shaped pores due to interparticle aggregation.

The specific surface area of the supporting LaNiO<sub>3</sub> is rather low (**Table 1**): 7.6 m<sup>2</sup>/g; a slight increase seems to be observed in the nanocomposite characterized by a higher copper amount. The pore volume is 0.027 cc/g in the supporting LaNiO<sub>3</sub> and increases

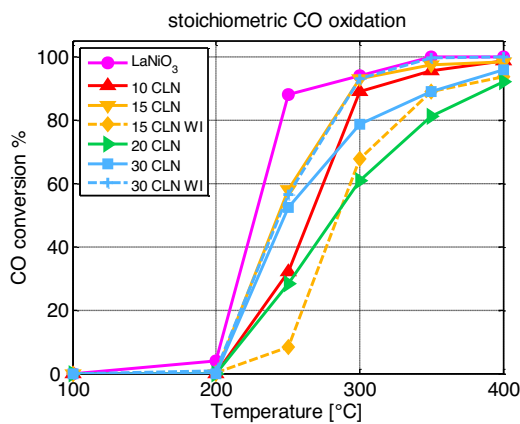


**Fig. 5.** CO conversion in  $\text{CO} + 1/2\text{O}_2$  stoichiometric oxidation reaction, measured from RT to  $400^\circ\text{C}$ , for  $\text{LaNiO}_3$  and for the  $\text{Cu}@\text{LaNiO}_3$  (CLN) samples obtained by ADP and WI as a function of the increasing copper amount.

to 0.039 cc/g as a consequence of copper deposition. The pore size dimension, in contrast, is almost constant. Combining with the results above, it can be concluded that the copper particles deposited on the materials are mainly on the support's surface rather than within the pores.

### 3.5. Catalytic tests

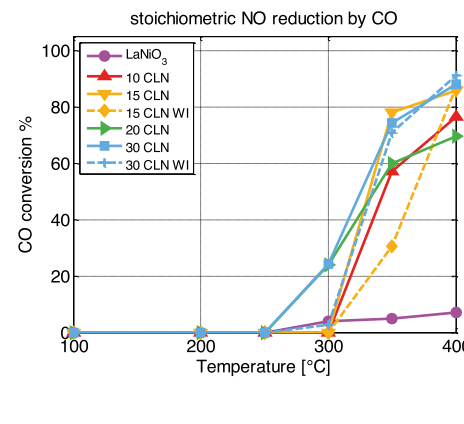
#### 3.5.1. Catalytic activity in CO oxidation and NO reduction

The activity of  $\text{LaNiO}_3$  in CO oxidation (Fig. 5) is not remarkably affected by CuO deposition on the catalyst. The relevant effect is a shift in the light-off temperature of the catalyst, about 50 °C higher after copper oxide deposition. 15 CLN and 30 CLN seem to have a lower  $T_{50}$  (50% conversion temperature), which is approximately 250 °C. At 400 °C all the copper deposited samples show a similar behaviour with an almost total conversion of CO.

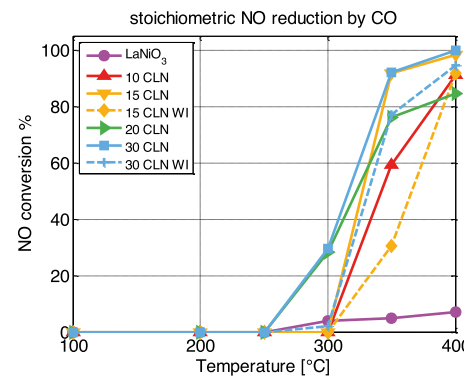
The slightly lower catalytic activity of the 20 CLN sample could be related to the lower amount of perovskitic oxygen of 20 CLN sample with respect to the hydroxylation/carbonatation component. On the other hand, copper deposition appears to improve significantly the activity of  $\text{LaNiO}_3$  in reduction, lowering the temperature required to observe measurable conversion and increasing yield to  $\text{N}_2$  (Fig. 6). Both the effects are proportional to the amount of deposited copper. The first breakthrough is evident in 20 CLN and 30 CLN samples that show activation between 250 °C and 300 °C, about 50 °C lower than 10 CLN and 15 CLN samples. However, only 30 CLN and 15 CLN samples reach a total NO conversion at 400 °C; this is consistent with EDX quantitative analysis: both surface and bulk composition reveal a copper content for these samples that is higher than the nominal. The other progress related to the deposited copper is the enhanced yield to  $\text{N}_2$  (Fig. 6c), that demonstrates an almost total conversion of NO to nitrogen; the difference is correlated to small amounts of  $\text{N}_2\text{O}$ , detected from FTIR measurements, especially at low temperature (See Supplementary material).

Taking into consideration the reaction mechanism [91] the perovskite has to be able to promote the CO oxidation (and thus the oxygen mobility/exchange) and the dissociative interaction of NO. In addition, the oxygen exchange between these species is likely to happen with the intervention of the surface anion vacancies.

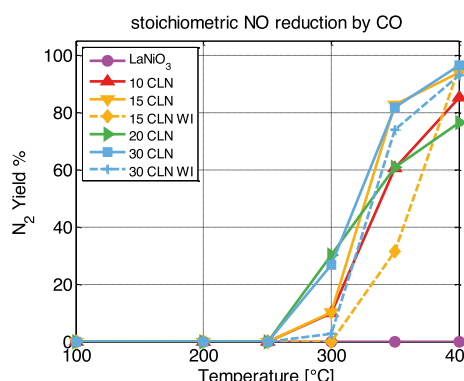
At low temperatures the Rate Determining Step (RDS) of the catalytic reduction of NO by CO is the activation of NO with the formation of  $\text{N}_2$  and/or  $\text{N}_2\text{O}$  [92]. The first step in the perovskite catalysed NO reduction, is the interaction of NO with a lattice oxygen vacancy which provides enough energy for the N–O bond breakage [92,93]. In this case, in contrast, no significant amount



a)



b)



c)

**Fig. 6.** CO conversion (a), NO conversion (b) and  $\text{N}_2$  yield (c) in CO-assisted NO reduction, from RT to  $400^\circ\text{C}$ , for  $\text{LaNiO}_3$  and for the  $\text{Cu}@\text{LaNiO}_3$  (CLN) samples obtained by ADP and WI as a function of the increasing copper amount.

of vacancies are expected to be present whereas, as confirmed by XPS, copper is distributed on surface. Copper cations are expected to coordinate two NO molecules forming a dinitrosyl specie that decomposes forming  $\text{N}_2$  and/or  $\text{N}_2\text{O}$  [93].

The NO dissociation can also involve the formation of the dimeric species ( $\text{N}_2\text{O}_2$ ) as intermediate; in this case the formation of  $\text{N}_2\text{O}$  is much easier only involving a N–O bond breaking whereas the formation of  $\text{N}_2$  should result from two bonds cleavages. It is interesting to observe that, as summarized by Centi et al. [93] the presence of Cu(II) and/or Cu(I) appears to deeply affect the formation of dinitrosyl species. Consistently, the TPR results suggest for copper an active role in the reduction reaction. Once formed the  $\text{N}_2\text{O}$  can decompose to  $\text{N}_2$  and  $\text{O}_2$  or react with the CO, giving rise to  $\text{N}_2$  and  $\text{CO}_2$ . In line with this mechanism the role of copper can be explained with the capability to coordinate NO and a minimum amount of copper cations on the surface is necessary to activate the reaction at lower temperature. The different behaviour observed, at lower temperature, between the samples obtained by ADP and WI,

suggest that the copper oxide particles dimension and distribution contribute to activate NO at lower temperature.

The comparison between the samples prepared by ADP and the ones prepared by WI revealed that WI synthesis results in an apparently higher activation energy, that delays the onset of reactivity by some tens of degrees, still allowing almost complete conversion at 400 °C, comparable to the ADP samples. This effect is more pronounced for the 15 CLN sample, for which a remarkable difference in both CO and NO conversion and N<sub>2</sub> yield is observed at 350 °C. These evidences suggest that the same amount of copper deposited by ADP is more dispersed than in WI sample, hence it is more effective for reduction at lower temperatures. As a confirmation, the catalysts that became active at lower temperature are those for which the TEM and TPR suggested a higher number of more highly dispersed copper oxide.

### 3.5.2. Catalytic activity with realistic automotive exhaust mixture

Three catalysts of the entire set were also tested with a more complex gas mixture. LaNiO<sub>3</sub>, 15 CLN and 30 CLN were selected to investigate the influence of CuO deposition. The choice was based on samples with relevant differences in nominal CuO amount and which provided the most interesting activity with the simpler mixture. In particular the catalysts characterized by the higher difference in catalytic performance at lower temperature (300 °C) were preferred because the catalytic behaviour tends to be more uniform at higher temperatures. With respect to the tests of Figs. 5 and 6, the investigated temperature is increased up to 600 °C. Although the higher temperature may activate homogeneous reactions, particularly of the heaviest hydrocarbons, blank tests confirmed a negligible contribution, with this mixture, as reported in Ref. 47.

The two different complex mixtures used in the tests (Table 2, Section 2.4) aim at approximating a real automotive exhaust composition, including a large amount of steam and CO<sub>2</sub>. In the stoichiometric one, the oxygen required by the fuels (CO, H<sub>2</sub>, HC<sub>s</sub>) to achieve total oxidation is provided by both the O<sub>2</sub> fed and the O<sub>2</sub> expected from NO reduction. In case NO is not reduced, a small lack of O<sub>2</sub> may be effective.

On the other side, a distinct feature of the O<sub>2</sub> substoichiometric condition is that oxygen can be totally consumed. It has been observed with all the samples presented in this work, at approx. 400 °C, feeding a fuel-rich mixture. Above this temperature, the catalyst will support oxidation in its entrance region, depleting all the O<sub>2</sub> available, while the remaining catalyst is exposed to a mixture that contains oxidation products (CO<sub>2</sub> and H<sub>2</sub>O, in addition to the large amount already fed) and unconverted CO and HC<sub>s</sub>. These are conditions where reforming, cracking, and water-gas shift reactions occur. Ni can be effective in some of these reactions. The detailed activity of each catalyst is described in Figs. 7–13.

In Fig. 7 the results for the CO conversion achieved at different inlet temperatures are shown for LaNiO<sub>3</sub>, 15 CLN and 30 CLN. First, Fig. 7a shows that the onset of the reactions at stoichiometric O<sub>2</sub> is consistent with the results of the simpler CO + O<sub>2</sub> stoichiometric mixture (Fig. 5), occurring at approximately 200 °C. However, the increase of conversion by raising the temperature appears significantly weaker. It is another indication of the interactions with the other species in the complex mixture, possibly leading to competitive adsorption/desorption mechanisms on catalysts surface. Comparing the activity when varying the CuO amount, Fig. 7a, it can be observed that the rate of CO oxidation is markedly enhanced by copper deposition, lowering the temperature to achieve the same conversion obtained by LaNiO<sub>3</sub> by approx. 70 °C on both nanocomposite samples. However, the enhancement seems to be independent from the amount of deposited copper oxide.

In Fig. 7b we clearly recognize the effect of reforming reactions, in shortage of O<sub>2</sub> available. At high temperatures (>400 °C) CO pro-

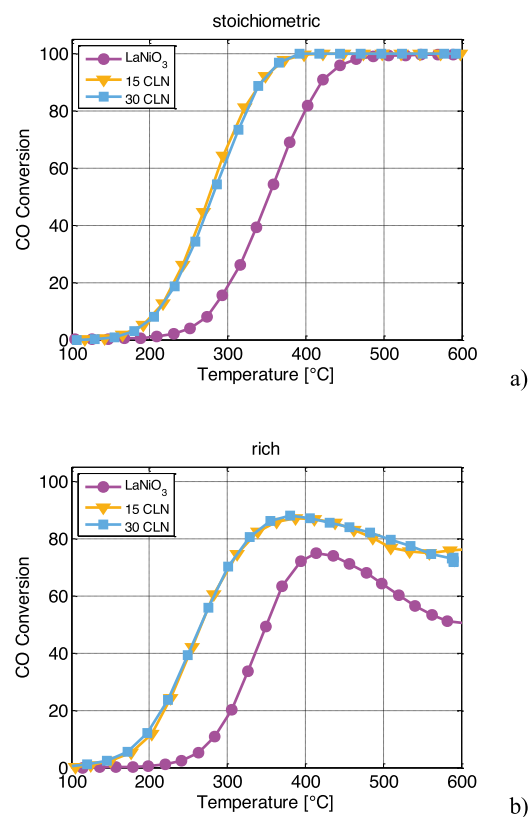
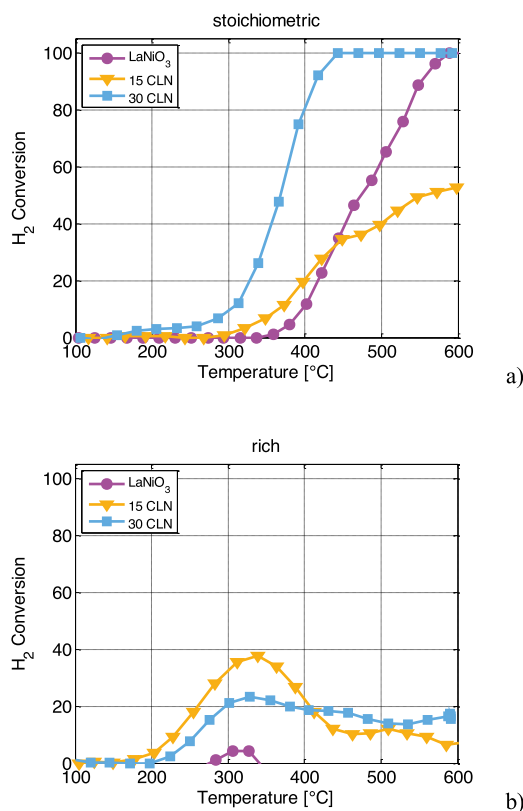


Fig. 7. CO conversion as a function of temperature, using realistic automotive exhaust mixture with stoichiometric (a) or understoichiometric O<sub>2</sub> (b), for LaNiO<sub>3</sub> and Cu@LaNiO<sub>3</sub> samples (CLN) obtained by ADP.

duction becomes competitive with its consumption, resulting in a drop of conversion. Again, CuO further improves the oxidation of CO, lowering by 100 °C its ignition, both on 15 CLN and 30 CLN, compared to the bare LaNiO<sub>3</sub>. It is confirmed that the amount of CuO does not improve further the CO reactivity. CuO also mitigates the relative importance of reforming reactions.

Concerning H<sub>2</sub>, also its oxidation in stoichiometric conditions appears to be facilitated by a significant (30%) CuO amount, as can be seen in Fig. 8a. It takes place at approx. 150 °C lower temperature on 30 CLN, allowing total H<sub>2</sub> combustion to be achieved at quite low temperature. The effect is less evident at the smaller CuO loading (15 CLN), where total conversion could not be achieved even at high temperature, reaching a maximum conversion of approx. 50% at 550 °C, notwithstanding the availability of O<sub>2</sub> (see Fig. 13a). In Fig. 8b, we see that a fuel-rich mixture facilitates reforming reactions on LaNiO<sub>3</sub>, competing with the oxidation, up to the temperature where they prevail on the consumption, leading to negative conversions (i.e. production of H<sub>2</sub>) above 350 °C, down to a minimum of -25% (not shown in Fig. 8b). Similarly to the indication of CO, 15 CLN and 30 CLN limit the reforming, so that production of both CO and H<sub>2</sub> is smaller on Cu@LaNiO<sub>3</sub> samples. Results are consistent with a lower availability of Ni on the catalytic surface, after CuO deposition, as suggested by XPS analysis.

The oxidation of C<sub>3</sub>H<sub>6</sub> at stoichiometric O<sub>2</sub>, Fig. 9a, begins at nearly 280 °C for all the three samples in stoichiometric mixture. The activity is almost independent from CuO loading, with a slight decrease at larger CuO amount. On the contrary, at fuel-rich conditions, Fig. 9b, the deposited CuO significantly lowers the temperature required to activate the C<sub>3</sub>H<sub>6</sub> oxidation, from 300 °C of LaNiO<sub>3</sub> to approx. 170 °C, for both CuO-loaded catalysts. Further, the high temperature is very effective in its conversion, also supported by its reforming, but the influence of the amount of CuO appears irrelevant.



**Fig. 8.**  $\text{H}_2$  conversion as a function of temperature, using realistic automotive exhaust mixture with stoichiometric (a) or understoichiometric  $\text{O}_2$  (b), for  $\text{LaNiO}_3$  and  $\text{Cu@LaNiO}_3$  samples (CLN) obtained by ADP.

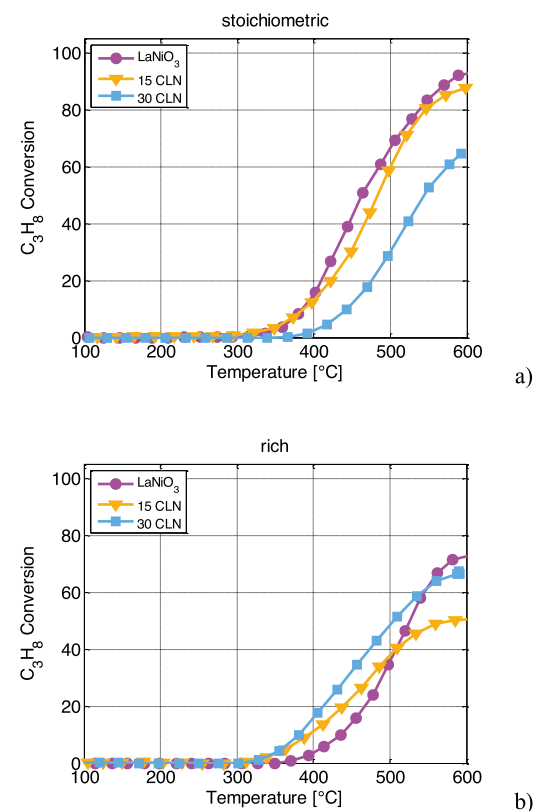


**Fig. 10.**  $\text{C}_3\text{H}_8$  conversion as a function of temperature, using realistic automotive exhaust mixture with stoichiometric (a) or understoichiometric  $\text{O}_2$  (b), for  $\text{LaNiO}_3$  and  $\text{Cu@LaNiO}_3$  samples (CLN) obtained by ADP.

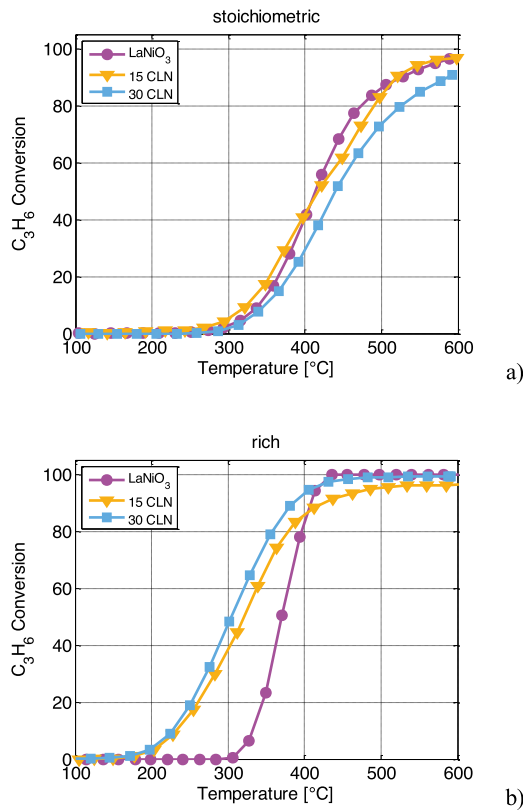


**Fig. 9.**  $\text{C}_3\text{H}_6$  conversion as a function of temperature, using realistic automotive exhaust mixture with stoichiometric (a) or understoichiometric  $\text{O}_2$  (b), for  $\text{LaNiO}_3$  and  $\text{Cu@LaNiO}_3$  samples (CLN) obtained by ADP.

**Fig. 10a** shows that CuO reduces the reactivity in propane oxidation as well, in the stoichiometric mixture, more clearly than propene. Apparently, the effect requires a larger amount of CuO to be evident, whereas 15 CLN is only slightly less active than  $\text{LaNiO}_3$ . To achieve the same conversion, 30 CLN requires a temperature approx. 100 °C higher than  $\text{LaNiO}_3$ . However, the oxidation of saturated C3 is comparatively more difficult anyway.

In fuel-rich conditions, **Fig. 10b**, we confirm the coexistence of reforming reactions to consume propane, extremely clear when oxygen is completely depleted (above 400 °C, see **Fig. 13b**). This chemical route appears easier on  $\text{LaNiO}_3$ , based on the propane conversion at the maximum temperature achieved in the tests, (at 600 °C it is approx. 75%, that decreases to 65% and 50% on 15 CLN and 30 CLN respectively). However, the limited conversion achieved even at the highest temperature, and the smaller effect of raising the temperature on propane consumption suggest that propane reforming requires a higher activation energy, i.e. it follows oxidation. We conclude that CuO deposition slightly facilitates the propane oxidation, taking place at lower temperature, but has negative influence on reforming.

Similarly to CO, also the oxidation of  $\text{CH}_4$  is supported by the presence of CuO, still remaining extremely low. At stoichiometric conditions, **Fig. 11a**, methane conversion reaches 12% at 600 °C on 15 CLN, a small but not negligible value. The activity is not replicated on 30 CLN, suggesting the existence of an optimum amount of doping for  $\text{CH}_4$  oxidation. In fuel-rich conditions, **Fig. 11b**, we observe a slightly higher conversion of methane, attributed to concurrent reforming, rather than combustion, being  $\text{O}_2$  totally consumed at this temperature.  $\text{CH}_4$  conversions of 12% and 20% are achieved with 15 CLN and 30 CLN respectively.

In **Fig. 12** the activity of the three samples in NO decomposition is shown. NO is negligibly activated if  $\text{O}_2$ -rich conditions prevail,

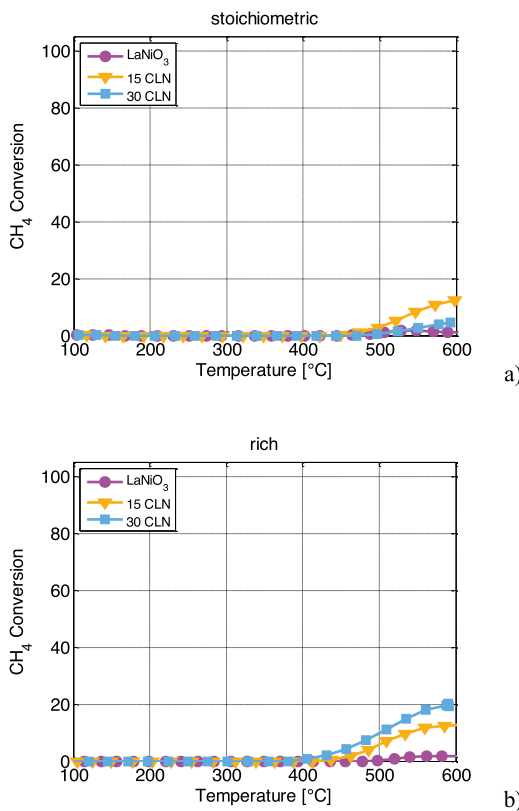


**Fig. 11.** CH<sub>4</sub> conversion as a function of temperature, using realistic automotive exhaust mixture with stoichiometric (a) or understoichiometric O<sub>2</sub> (b), for LaNiO<sub>3</sub> and Cu@LaNiO<sub>3</sub> samples (CLN) obtained by ADP.

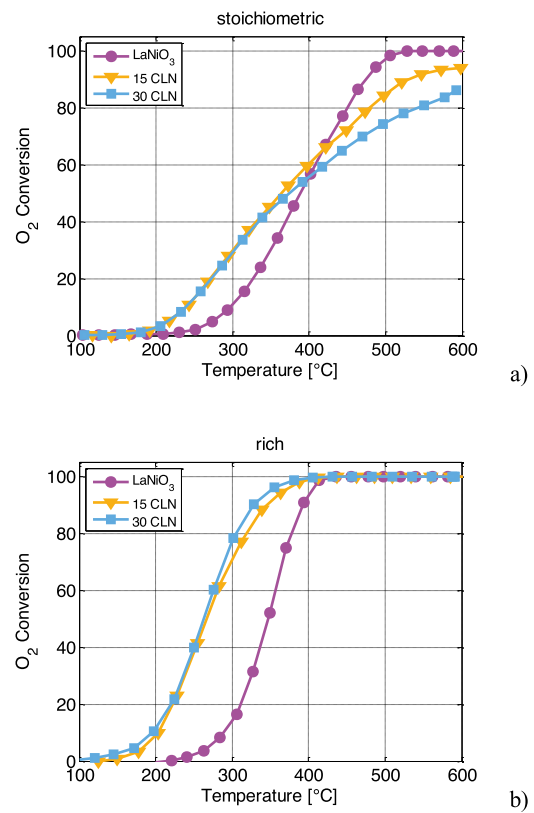


**Fig. 13.** O<sub>2</sub> conversion as a function of temperature, using realistic automotive exhaust mixture with stoichiometric (a) or understoichiometric O<sub>2</sub> (b) for LaNiO<sub>3</sub> and Cu@LaNiO<sub>3</sub> samples (CLN) obtained by ADP.

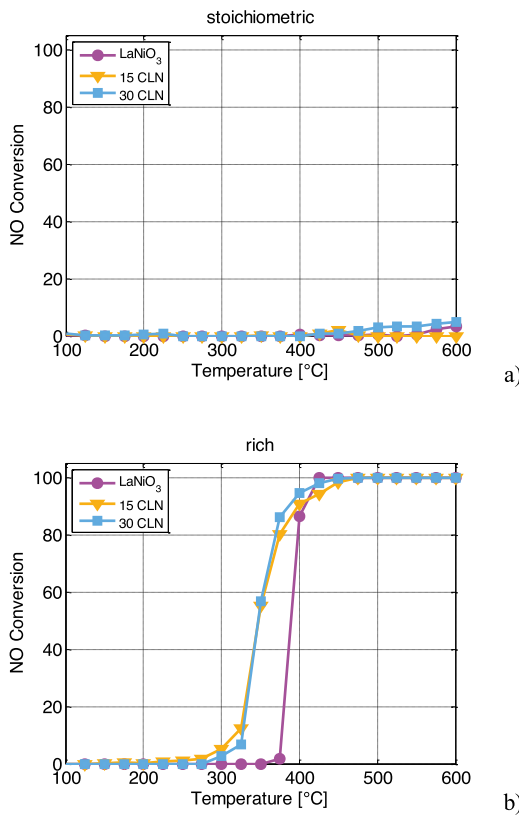


**Fig. 12.** NO conversion as a function of temperature, using realistic automotive exhaust mixture with stoichiometric (a) or understoichiometric O<sub>2</sub> (b), for LaNiO<sub>3</sub> and Cu@LaNiO<sub>3</sub> samples (CLN) obtained by ADP.

**Fig. 12a**, independently from any CuO loading. Neither CO nor H<sub>2</sub> assisted NO reduction occurs, when some O<sub>2</sub> is available. Conversely, the activity with O<sub>2</sub>-lean mixture is totally different, as shown in **Fig. 12b**. Bare LaNiO<sub>3</sub> appears very active in NO reduction: T<sub>10</sub> (10% conversion temperature) temperature is 380 °C and complete conversion is achieved at approx. 420 °C. In the nanocomposites the activity is further improved: 15 CLN T<sub>10</sub> is 320 °C, followed by 30 CLN with approx. 330 °C, lowering respectively of 60 °C and 50 °C that obtained with LaNiO<sub>3</sub>. It is worth noting that the activity in NO reduction is measured even in the presence of unreacted O<sub>2</sub> (**Fig. 13b**), considered the actual obstacle for NO reduction.

Finally, **Fig. 13** shows the conversions of O<sub>2</sub> in all the cases presented so far, and provides overall information about the behaviour of the catalysts with the two different mixtures. The O<sub>2</sub> consumption onset indicates the minimum temperature at which the catalyst is active, that is approx. 200 °C for all the samples in stoichiometric conditions, **Fig. 13a**. Between 200 °C and 400 °C, the consumption of O<sub>2</sub> is higher in 15 CLN and 30 CLN confirming that they support a higher activity in oxidation. Above 400 °C, with LaNiO<sub>3</sub> oxidation of HCs, H<sub>2</sub> and CO is overall higher than the CuO nanocomposites and the available O<sub>2</sub> is totally consumed, not being supplemented by NO reduction, negligibly activated (**Fig. 12a**). The lack of O<sub>2</sub> at high temperatures could be a limiting factor for HCs complete oxidation on LaNiO<sub>3</sub>.

Above 500 °C the total consumption of O<sub>2</sub> in the first part of the bed together with residual H<sub>2</sub> determines a region where reducing conditions occur [94], possibly supporting the onset of a small NO conversion, shown by the data. The consumption of oxygen with a fuel-rich mixture is reported in **Fig. 13b**. It is evident that nanocomposites with CuO enhance the activity of LaNiO<sub>3</sub>, lowering the light-off temperature from approx. 200 °C of LaNiO<sub>3</sub> to 150 °C of the nanocomposites. Still, the O<sub>2</sub> produced by NO reduction is not

sufficient to affect the reactions, being totally consumed by excess of fuels. The improvements obtained in doping  $\text{LaNiO}_3$  with  $\text{CuO}$ , resulting in lower light-off temperatures, are a remarkable result of these new materials, as seen from the ignition temperatures of  $\text{CO}$ ,  $\text{NO}$  and  $\text{C}_3\text{H}_6$ . However, a proportional correlation between catalytic activity and  $\text{CuO}$  amount is often lacking, showing similar effects when loaded in both low and high amount. This suggests the possibility to optimize the amount of doping without decreasing the performances of the materials.

Further work is in course to go deeper into the difference and try to fill the gap between model and real catalyst reactivity.

### 3.5.3. Catalytic activity after aging

The catalytic activity before and after the thermal aging treatment (3 h at  $700^\circ\text{C}$  followed by 3 h at  $800^\circ\text{C}$ ) is reported for the 20 CLN sample and compared in Fig. 14 for each component of the reacting mixture. The feed mixture is the synthetic realistic automotive exhaust, stoichiometric.

Overall, the aging treatment causes a slight loss in catalytic activity. It can be observed in the consumption of  $\text{O}_2$ , that for aged 20 CLN is lower (up to 10%) than for fresh sample. More specifically,  $\text{CO}$ ,  $\text{C}_3\text{H}_6$  and  $\text{NO}$  reaction rates (observed by the conversion achieved within the same residence time) decrease after high-temperature treatment. Interestingly,  $\text{H}_2$  and  $\text{C}_3\text{H}_8$  oxidation rate appears barely affected by aging.  $\text{CH}_4$  combustion is not activated in both cases.

## 4. Conclusions

In this contribution several nanocomposites have been obtained by depositing  $\text{CuO}$  on the surface of a  $\text{LaNiO}_3$  perovskite using a well optimized ammonia driven deposition precipitation method.

The XRD patterns reveal the presence of cubic  $\text{CuO}$ . No shift of the signals due to the perovskite is observed as a function of  $\text{CuO}$  amount suggesting that copper does not enter the perovskitic cell.

XPS suggests that the  $\text{CuO}$  deposition deeply affects the surface segregation phenomena: in particular Lanthanum was observed to be surface segregate in  $\text{LaNiO}_3$ , but this phenomenon is not evident anymore after deposition. Moreover, the  $\text{Cu}/\text{La}$  surface atomic ratio is not linear with the nominal amount of Cu, suggesting some kind of diffusion into the powder bulk. Copper oxide is deposited both in highly dispersed and more compact particles and the deposition significantly affects the  $\text{LaNiO}_3$  reduction.

$\text{LaNiO}_3$ , and nano-composites activity has been tested both on simple  $\text{CO} + \text{NO}$  and  $\text{CO} + \text{O}_2$  stoichiometric mixtures. The activity of  $\text{LaNiO}_3$ , 15 CLN, and 30 CLN was also investigated using realistic automotive exhaust mixtures, stoichiometric and fuel-rich. Simple mixtures indicated that copper deposition improves significantly the NO reduction ability by  $\text{CO}$  on  $\text{LaNiO}_3$ , increasing NO reduction to  $\text{N}_2$  and lowering the temperature required to yield measurable conversion. The activity of  $\text{LaNiO}_3$  in  $\text{CO}$  oxidation in the absence of other species does not appear to be significantly affected by copper deposition. The complex mixture, including 10%  $\text{H}_2\text{O}$ , shows that deposition of  $\text{CuO}$  enhances the capability of  $\text{LaNiO}_3$  in  $\text{CO}$  ox-

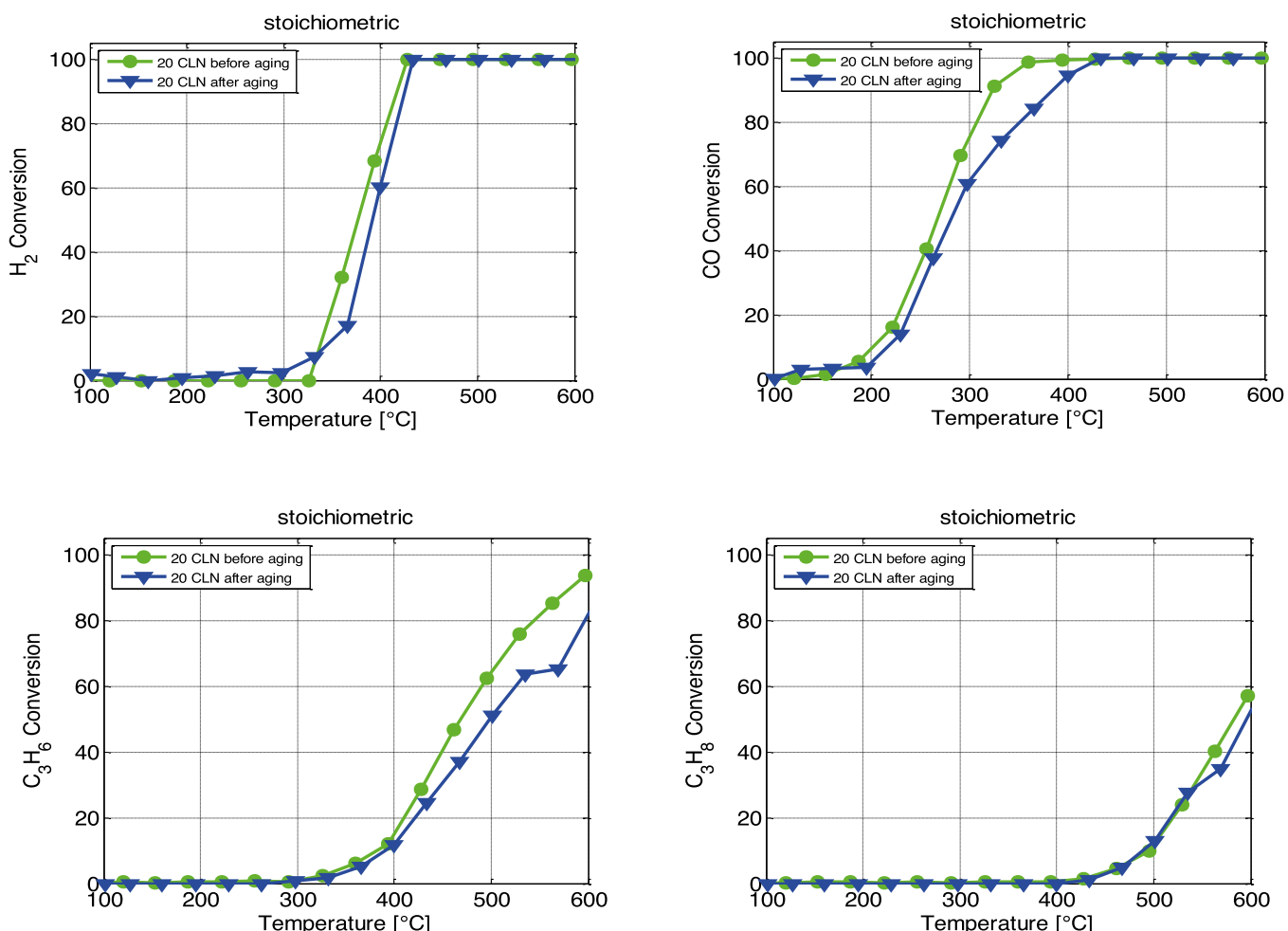


**Fig. 14.** Comparison between the activity before (green lines) and after (blue lines) aging for 20 CLN sample, in terms of each reactants conversion. (For interpretation of the references to colour in this figure legend, the reader is referred to the web version of this article.)

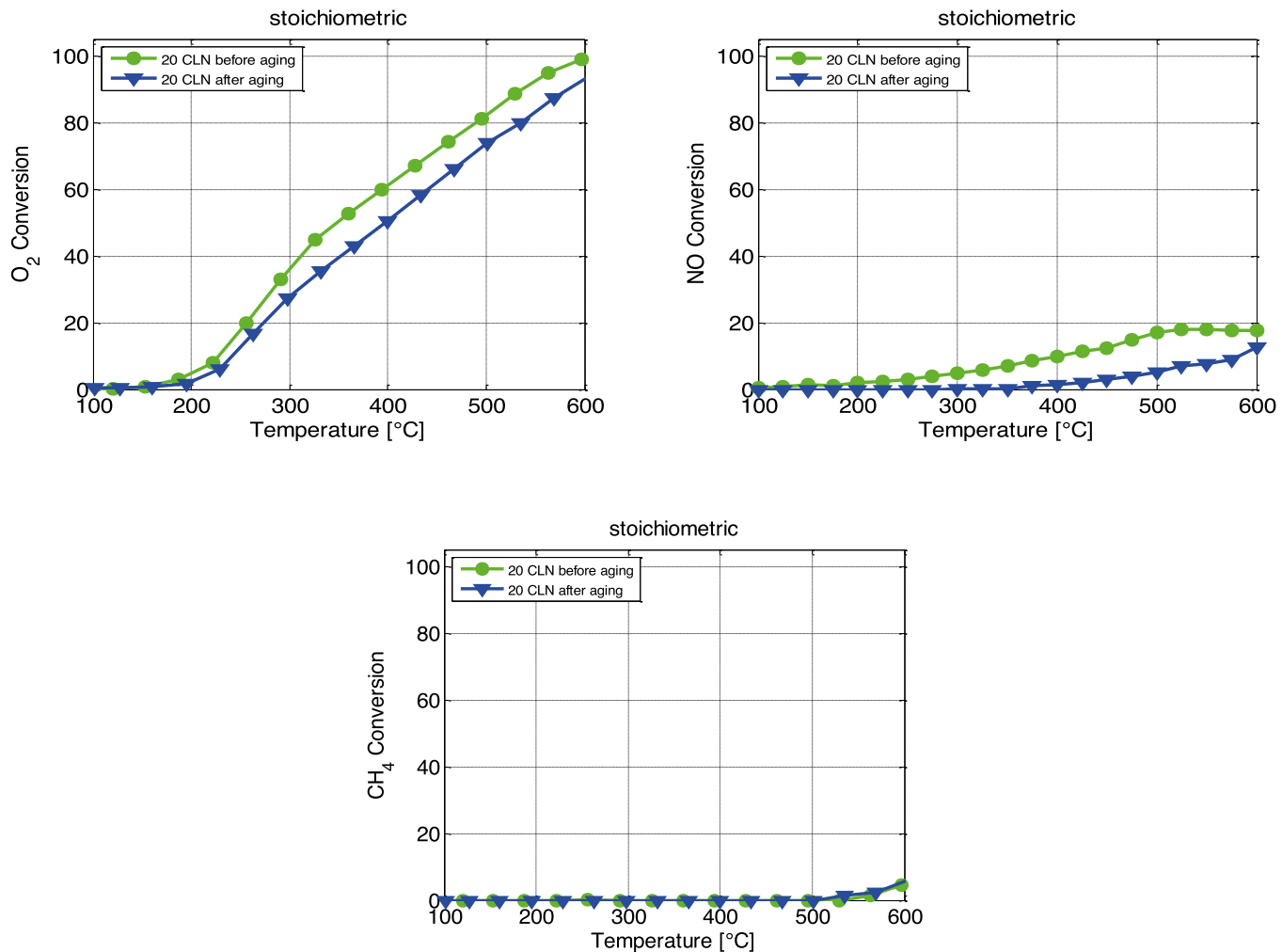


Fig. 14. (Continued)

dation, almost independently from the amount of deposition, in stoichiometric mixtures. Conversely, CuO slightly limits the oxidation activity of C<sub>3</sub>H<sub>8</sub>, without being significantly useful in C<sub>3</sub>H<sub>6</sub> and CH<sub>4</sub> oxidation. In fuel rich mixture CuO improve the oxidation activity, thus limiting the reforming reactions. Notably, it significantly improves the NO decomposition, but sub-stoichiometric O<sub>2</sub> is still required. The thermal aging carried out at stoichiometric conditions, with a real mixture (including 10% H<sub>2</sub>O), does not cause a significant drop of activity. The most affected reactions are the oxidation of CO, between 300 and 400 °C, and the reduction of NO, above 300 °C, with an average maximum activity drop of 10%.

#### Acknowledgment

The research work was conducted in the frame of the EU-FP7 project Next-Gen-Cat ('Development of Next Generation Cost Efficient Automotive Catalysts'; project n° 280890). We thank Dr. Annalisa Sandon for the ICP measurements and Lab of Microscopy of Dept. of Biology, University of Padova for TEM images.

#### Appendix A. Supplementary data

Supplementary data associated with this article can be found, in the online version, at <http://dx.doi.org/10.1016/j.apcatb.2017.02.064>.

#### References

- [1] H.S. Gandhi, G.W. Graham, R.W. McCabe, J. Catal. 216 (2003) 433–442.
- [2] W.F. Libby, Science 171 (1971) 499–500.
- [3] K.-H. Lin, C.-B. Wang, S.-H. Chien, Int. J. Hydrogen Energy 38 (2013) 3226–3232.
- [4] A.A.A. da Silva, L.O.O. da Costa, L.V. Mattos, F.B. Noronha, Catal. Today 213 (2013) 25–32.
- [5] J. Guo, H. Lou, Y. Zhu, X. Zheng, Mater. Lett. 57 (2003) 4450–4455.
- [6] C. Batiot-Dupeyrat, G. Valderrama, A. Meneses, F. Martinez, J. Barrault, J.M. Tatibouët, Appl. Catal. A: Gen. 248 (2003) 143–151.
- [7] G. Valderrama, M.R. Goldwasser, C. Urbina de Navarro, J.M. Tatibouët, J. Barrault, C. Batiot-Dupeyrat, F. Martínez, Catal. Today 107–108 (2005) 785–791.
- [8] C. Batiot-Dupeyrat, G.A. Sierra Gallego, F. Mondragón, J. Barrault, J.M. Tatibouët, Catal. Today 107–108 (2005) 474–480.
- [9] S.M. Lima, J.M. Assaf, M.A. Peña, J.L.G. Fierro, Appl. Catal. A: Gen. 311 (2006) 94–104.
- [10] G.A. Sierra Gallego, F. Mondragón, J. Barrault, J.M. Tatibouët, C. Batiot-Dupeyrat, Appl. Catal. A: Gen. 311 (2006) 164–171.
- [11] M.E. Rivas, J.L.G. Fierro, M.R. Goldwasser, E. Pietri, M.J. Pérez-Zurita, A. Griboval Constant, G. Leclercq, Appl. Catal. A: Gen. 344 (2008) 10–19.
- [12] G.C. de Araujo, S.M. de Lima, J.M. Assaf, M.A. Peña, J.L.G. Fierro, M.C. Rangel, Catal. Today 133–135 (2008) 129–135.
- [13] G.A. Sierra Gallego, C. Batiot-Dupeyrat, J. Barrault, E. Florez, F. Mondragón, Appl. Catal. A: Gen. 334 (2008) 251–258.
- [14] G. Valderrama, A. Kiennemann, M.R. Goldwasser, Catal. Today 133–135 (2008) 142–148.
- [15] G.S. Gallego, J. Gallego Marín, C. Batiot-Dupeyrat, J. Barrault, F. Mondragón, Appl. Catal. A: Gen. 369 (2009) 97–103.
- [16] J. Gallego, C. Batiot-Dupeyrat, J. Barrault, F. Mondragón, Energy Fuels 23 (2009) 4883–4886.
- [17] R. Pereñiguez, V.M. González-DelaCruz, J.P. Holgado, A. Caballero, Appl. Catal. B: Environ. 93 (2010) 346–353.

- [18] G.R. Moradi, R. Rahmazadeh, S. Sharifnia, Chem. Eng. J. 162 (2010) 787–791.
- [19] R. Pereñiguez, V.M. González-DelaCruz, A. Caballero, J.P. Holgado, Appl. Catal. B. Environ. 123–124 (2012) 324–332.
- [20] G.R. Moradi, M. Rahmazadeh, Catal. Commun. 26 (2012) 169–172.
- [21] A. Jahangiri, H. Pahlavanzadeh, H. Aghabozorg, Int. J. Hydrogen Energy 37 (2012) 9977–9984.
- [22] M.M. Nair, S. Kaliaguine, F. Kleitz, ACS Catal. 4 (2014) 3837–3846.
- [23] G.R. Moradi, M. Rahmazadeh, F. Khosravian, J. CO<sub>2</sub> Util. 6 (2014) 7–11.
- [24] B.S. Barros, Y.-J. Su, K.-L. Pan, M.-B. Chang, Int. J. Hydrogen Energy 39 (2014) 4917–4925.
- [25] B.S. Barros, J. Kulesza, D.M. de Araújo Melo, A. Kienneman, Mater. Res. 18 (2015) 732–739.
- [26] J.R. Mawdsley, T.R. Krause, Appl. Catal. A: Gen. 334 (2008) 311–320.
- [27] S.M. de Lima, A.M. da Silva, L.O.O. da Costa, J.M. Assaf, G. Jacobs, B.H. Davis, L.V. Mattos, F.B. Noronha, Appl. Catal. A: Gen. 377 (2010) 181–190.
- [28] L. Huang, F. Zhang, N. Wang, R. Chen, A.T. Hsu, Int. J. Hydrogen Energy 37 (2012) 1272–1279.
- [29] U. Oemar, P.S. Ang, K. Hidajat, S. Kawi, Int. J. Hydrogen Energy 38 (2013) 5525–5534.
- [30] K. Soongprasit, D. Aht-Ong, V. Sricharoenchaikul, D. Atong, Curr. Appl. Phys. 12 (2012) S80–S88.
- [31] H. Provendier, C. Petit, C. Estournès, S. Libs, A. Kiennemann, Appl. Catal. A: Gen. 180 (1999) 163–173.
- [32] C.R.B. Silva, L. da Conceição, N.F.P. Ribeiro, M.M.V.M. Souza, Catal. Commun. 12 (2011) 665.
- [33] G.C. de Araújo, S. Lima, M.C. Rangel, V. La Parola, M.A. Peña, J.L.G. Fierro, Catal. Today 107–108 (2005) 906.
- [34] L.D. Vella, J.A. Villoria, S. Specchia, N. Mota, J.L.G. Fierro, V. Specchia, Cat. Today 171 (2011) 84–96.
- [35] S.-K. Liu, Y.-C. Lin, Catal. Today 237 (2014) 62–70.
- [36] C.A. Franchini, W. Aranzaez, A.M. Duarte de Farias, G. Pecchi, M.A. Fraga, Appl. Catal. B: Environ. 147 (2014) 193–202.
- [37] G. Wu, S. Li, C. Zhang, T. Wang, J. Gong, Appl. Catal. B. Environ. 144 (2014) 277–285.
- [38] T. Vaz, A.V. Salker, Mater. Sci. Eng. B 143 (2007) 81–84.
- [39] S.S. Maluf, E.M. Assaf, Catal. Commun. 12 (2011) 703–706.
- [40] K. Rida, M.A. Peña, E. Sastre, A. Martínez-Arias, J. Rare Earths 30 (2012) 210–216.
- [41] M. Navarro, M.A. Peña, J.L.G. Fierro, Chem. Rev. 107 (2007) 3952–3991.
- [42] C.-Y. Lu, W.-C. Chang, M.-Y. Wey, Mater. Chem. Phys. 141 (2013) 512–518.
- [43] S. Zeng, Y. Wang, S. Ding, J.J.H.B. Sattler, E. Borodina, L. Zhang, B.M. Weckhuysen, H. Su, J. Power Sources 256 (2014) 301–311.
- [44] C. Tang, J. Sun, X. Yao, L. Liu, C. Ge, F. Gao, L. Dong, Appl. Catal. B: Environ. 146 (2014) 201–212.
- [45] A.K. Ahmed, A.A. Zuhairi, M.A. Rahman, Renewable Sustainable Energy Rev. 44 (2015) 508–518.
- [46] S.G. Jadava, P.D. Vaidya, B.M. Bhanageb, J.B. Joshi, Chem. Eng. Res. Des. 92 (2014) 2557–2567.
- [47] A. Glisenti, M. Pacella, M. Guiotto, M.M. Natile, P. Canu, Appl. Catal. B: Environ. 180 (2016) 94–105.
- [48] S. Sá, H. Silva, L. Brandão, J.M. Sousa, A. Mendes, Appl. Catal. B Environ. 99 (2010) 43–57.
- [49] G. Busca, T. Montanari, C. Resini, G. Ramis, U. Costantino, Catal. Today 143 (2009) 2–8.
- [50] B. Frank, F.C. Jentoft, H. Soerijanto, J. Kröhnert, R. Schlögl, R. Schomäcker, J. Catal. 246 (2007) 177–192.
- [51] J. Agrell, M. Boutonnet, J.L.G. Fierro, Appl. Catal. A Gen. 253 (2003) 213–223.
- [52] M. Manzoli, A. Chiorino, F. Bocuzzi, Appl. Catal. B Environ. 57 (2004) 201–209.
- [53] M. Turco, G. Bagnasco, U. Costantino, F. Marmottini, T. Montanari, G. Ramis, G. Busca, J. Catal. 228 (2004) 43–55.
- [54] T. Valdés-Solís, G. Marbán, A.B. Fuertes, Catal. Today 116 (2006) 354–360.
- [55] X. Hong, S. Ren, Int. J. Hydrogen Energy 33 (2008) 700–708.
- [56] N. Iwasa, N. Takezawa Bull, Chem. Soc. Jpn. 64 (1991) 2619–2623.
- [57] F.J. Mariño, E.G. Cerrella, S. Duhalde, M. Jobbagy, M.A. Laborde, Int. J. Hydrogen Energy 23 (1998) 1095–1101.
- [58] S. Velu, N. Satoh, C.S. Gopinath, K. Suzuki, Catal. Lett. 82 (2002) 145–152.
- [59] S. Velu, K. Suzuki, M.B. Vijayaraj, S. Barman, C.S. Gopinath, Appl. Catal. B Environ. 55 (2005) 287–299.
- [60] T. Nishiguchi, T. Matsumoto, H. Kanai, K. Utani, Y. Matsumura, W.-J. Shen, S. Imamura, Appl. Catal. A Gen. 279 (2005) 273–277.
- [61] O. Akdim, W. Cai, V. Fierro, H. Provendier, A. van Veen, W. Shen, C. Mirodatos, Top. Catal. 51 (2008) 22–38.
- [62] C.E.M. Garido, D.V. Cesar, Souza M.M.V.M, M. Schmal, Catal. Today 142 (2009) 252–257.
- [63] C.G. Alonso, A.C. Furtado, M.P. Cantão, O.A. Andreo dos Santos, N.R.C. Fernandes-Machado, Int. J. Hydrogen Energy 34 (2009) 3333–3341.
- [64] R. Guil-López, R.M. Navarro, M.A. Peña, J.L.G. Fierro, Int. J. Hydrogen Energy 36 (2011) 1512–1523.
- [65] L.-C. Chen, S.D. Lin, Appl. Catal. B Environ. 106 (2011) 639–649.
- [66] I. Rodriguez-Ramos, A. Guerrero-Ruiz, M.L. Rojas, J.L.G. Fierro, Appl. Catal. 68 (1991) 217–228.
- [67] X. Guo, A. Yin, W.L. Dai, Catal. Lett. 132 (2009) 22–27.
- [68] K. Ramanathan, S.H. Oh, Chem. Eng. Res. Des. 92 (2014) 350–361.
- [69] C. Marcilly, P. Courty, B. Delmon, J. Am. Ceram. Soc. 53 (1970) 56–57.
- [70] D.A. Shirley, Phys. Rev. B 5 (1972) 4709–4714.
- [71] J.F. Moulder, W.F. Stickle, P.E. Sobol, K.D. Bomben, Handbook of X-ray photoelectron spectroscopy, in: J. Chastain (Ed.), Physical Electronics, Eden Prairie, MN, 1992.
- [72] D. Briggs, J.C. Riviere, Practical Surface Analysis, in: D. Briggs, M.P. Seah (Eds.), Wiley, New York, 1983.
- [73] M. Guiotto, M. Pacella, G. Perin, A. Iovino, N. Michelon, M.M. Natile, A. Glisenti, P. Canu, Appl. Catal. A: Gen. 499 (2015) 146–157.
- [74] J. Li, L. Jia, W. Fang, J. Zeng, Int. J. Hydrogen Energy 35 (2010) 5270–5275.
- [75] M.M. Natile, F. Poletto, A. Galenda, A. Glisenti, T. Montini, L. De Rogatis, P. Fornasiero, Chem. Mater. 20 (2008) 2314–2327.
- [76] A. Galenda, M.M. Natile, V. Krishnan, H. Bertagnolli, A. Glisenti, Chem. Mater. 19 (2007) 2796–2808.
- [77] A. Galenda, M.M. Natile, L. Nodari, A. Glisenti, Appl. Catal. B Environ. 97 (2010) 307–322.
- [78] D.F. Mullica, H.O. Perkins, C.K.C. Lok, V. Young, J. Electron Microsc. 61 (1993) 337–355.
- [79] L.G. Tejuca, J.L.G. Fierro, Thermochim. Acta 147 (1989) 361–375.
- [80] M.F. Sunding, K. Hadidi, S. Diplas, O.M. Lovvik, T.E. Norby, A.E. Gunnaes, J. Electron Microsc. 184 (2011) 399–409.
- [81] NIST XPS Database 20, Version 3.4 (Web Version).
- [82] L. Qiao, X. Bi, EPL 93 (2011) 57002.
- [83] S. Damyanova, L. Daza, J.L.G. Fierro, J. Catal. 159 (1996) 150–161.
- [84] N.S. McIntyre, M.G. Cook, Anal. Chem. 47 (13) (1975) 2208–2213.
- [85] J.L.G. Fierro, Catal. Today 8 (1990) 153–174.
- [86] G.U. Kulkarni, C.N.R. Rao, M.W. Roberts, J. Phys. Chem 99 (1995) 3310–3316.
- [87] S.M. Lima, J.M. Assaf, Catal. Lett. 108 (2006) 63–70.
- [88] A. Glisenti, A. Galenda, M.M. Natile, Appl. Catal. A: Gen. 453 (2013) 102–112.
- [89] N. Tien-Thao, H. Alamdar, M.H. Zahedi-Niaki, S. Kaliaguine, Appl. Catal. A: Gen. 311 (2006) 204–212.
- [90] N. Tien Thao, H. Alamdar, S. Kaliaguine, J. Sol. State. Chem. 181 (2008) 2006–2019.
- [91] A.K. Ladavos, P.J. Pomonis, Appl. Catal. B 2 (1993) 27–47.
- [92] R. Zhang, A. Villanueva, H. Alamdar, S. Kaliaguine, J. Mol. Catal. A 258 (2006) 22–34.
- [93] G. Centi, S. Perathoner Appl. Catal. A: Gen. 132 (1995) 179–259.
- [94] D.D. Nogare, N.J. Degenstein, R. Horn, P. Canu, L.D. Schmidt, J. Catal. 277 (2011) 134–148.